Received: 10 September 2020 | Revised: 10 April 2021 | Accepted: 26 April 2021

DOI: 10.1002/mrm.28848

FULL PAPER

Magnetic Resonance in Medicine

Estimation and removal of spurious echo artifacts in single-voxel MRS using sensitivity encoding

Adam Berrington[1,2] | **Michal Považan**[1,3] | **Peter B. Barker**[1,3]

[1]Russell H. Morgan Department of Radiology and Radiological Science, Johns Hopkins University School of Medicine, Baltimore, Maryland, USA

[2]Sir Peter Mansfield Imaging Centre, School of Physics and Astronomy, University of Nottingham, Nottingham, United Kingdom

[3]F. M. Kirby Research Center for Functional Brain Imaging, Kennedy Krieger Institute, Baltimore, Maryland, USA

Correspondence
Adam Berrington, Sir Peter Mansfield Imaging Centre, School of Physics and Astronomy, University of Nottingham, Nottingham NG7 2RD, United Kingdom.
Email: adam.berrington@nottingham.ac.uk

Funding information
National Institutes of Health; Grant/Award No. P41EB015909

Purpose: In localized MRS, spurious echo artifacts commonly occur when unsuppressed signal outside the volume of interest is excited and refocused. In the spectral domain, these signals often overlap with metabolite resonances and hinder accurate quantification. Because the artifacts originate from regions separate from the target MRS voxel, this work proposes that sensitivity encoding based on receive-coil sensitivity profiles may be used to separate these signal contributions.

Methods: Numerical simulations were performed to explore the effect of sensitivity-encoded separation for unknown artifact regions. An imaging-based approach was developed to identify regions that may contribute to spurious echo artifacts, and tested for sensitivity-based unfolding of signal on six data sets from three brain regions. Spectral data reconstructed using the proposed method ("ERASE") were compared with the standard coil combination.

Results: The method was able to fully unfold artifact signals if regions were known a priori. Mismatch between estimated and true artifact regions reduced the efficiency of removal, yet metabolite signals were unaffected. Water suppression imaging was able to identify regions of unsuppressed signal, and ERASE (from up to eight regions) led to visible removal of artifacts relative to standard reconstruction. Fitting errors across major metabolites were also lower; for example, Cramér–Rao lower bounds of *myo*-inositol were 13.7% versus 17.5% for ERASE versus standard reconstruction, respectively.

Conclusion: The ERASE reconstruction tool was demonstrated to reduce spurious echo artifacts in single-voxel MRS. This tool may be incorporated into standard workflows to improve spectral quality when hardware limitations or other factors result in out-of-voxel signal contamination.

KEYWORDS
artifact removal, MRS, sensitivity encoding

1 | INTRODUCTION

Robust quantification of metabolite concentrations in single-voxel MRS of the brain is critically dependent on spectral quality. However, spectra are often observed to contain a number of artifacts,[1] which can lead to poor metabolite fitting, rejection of data sets based on quality criteria, and ultimately lowers the value of MRS for either research or clinical use. One commonly observed artifact is the spurious echo. In the spectral domain, the spurious echo manifests as an oscillatory or "beating" signal that spans a range of frequencies and often overlaps with metabolite resonances, and is also referred to as "ghosting artifact." A rigorous description of the origin of spurious echoes in MRS has been provided in terms of coherence pathways[2] and later k-space formalism within a PRESS localization sequence.[3] Essentially, spurious echoes arise from spins outside the voxel of interest that are excited at some point during the pulse sequence, such as due to imperfections in slice localization and coherence pathway selection, and then subsequently refocused by sequence elements or magnetic field gradients, generating an echo during signal reception. On Fourier transformation, this signal usually has a large first-order phase error, because it occurs at some variable time point in the FID. Given the sizeable concentration difference between water and metabolites in ^{1}H-MRS of brain (~10^4), the main contribution to the spurious echo artifact arises from regions of unsuppressed water signal,[3] although lipid resonances may also form spurious echoes.

It has been shown that when slice localization overlaps with air-filled cavities such as the frontal sinuses, the likelihood of observing spurious echo artifacts is increased.[4] Susceptibility differences at these air–water interfaces causes local B_0-field perturbation; hence, the water resonance can be shifted outside of the bandwidth of the water-suppression pulses. It has also been shown that localized higher-order shimming on small volumes of interest, as is commonly performed in MRS, generates an inhomogeneous B_0 field outside the volume of interest, which leads to regions of poor water suppression.[4]

A number of methods to remove these artifacts have been proposed. The use of outer-volume suppression pulses[5] can reduce the artifact intensity, as well as improved RF pulses for spatial localization (ie, minimizing excitation of out-of-voxel magnetization).[6,7] Phase-cycling schemes are used to eliminate unwanted coherence pathways and therefore reduce the presence of these artifacts; however, phase cycling is often performed with a small number of steps and is susceptible to subject motion. Crusher gradients also dephase unwanted coherences, although their efficacy may be limited if gradient strengths (and/or durations) are constrained by scanner hardware or sequence design.[8] An early study showed that the order of the slice-selective pulses (and hence cumulative crusher effect) could be used to minimize artifact intensity,[4] although the optimum order would likely vary depending on the voxel location and subject. Recent work has introduced mathematically optimized crusher schemes for different localization sequences.[9] In this way, unwanted coherences could be reduced. Nevertheless, crushing power is always limited by hardware constraints, acquisition geometry, and the minimum TE desired. Recently, a method to remove spurious echoes in MR spectra has examined the use of deep learning techniques, which were trained on simulated data sets.[10] The flexibility of applying deep learning to in vivo data sets, however, depends on the nature and extent of the training data.

The separation of aliased signal components based on their spatial position has been demonstrated in MRS using sensitivity-based techniques akin to SENSE acceleration.[11,12] One study showed that lipids aliased into a spectroscopic imaging grid could be separated from brain metabolite signals using coil sensitivity information.[13] In another study, after performing dual-voxel excitation, reconstruction of separate signals from the left and right hemispheres could be performed based on the sensitivity weighting of the receive coils, thereby accelerating the MRS acquisition by a factor of 2 compared with the sequential acquisition of spectra from each hemisphere.[14] It has also been previously proposed to add phase-encoding gradients to single-voxel MRS acquisitions followed by spatial Fourier transformation, to separate the desired region-of-interest signal from out-of-voxel artifacts.[15-17] The separation of spectral components from anatomical regions using receive coil information has also been shown using the SPLASH technique.[18]

In the current study, it was hypothesized that sensitivity information from multiple receive coils could be used to separate spurious echo artifacts from metabolite signal during a single-voxel acquisition, given that spurious echoes arise from regions outside of the volume of interest. A requirement for this method is that the location of the artifact region must be known in order to successfully separate it from the actual region of interest. Here, potential regions of artifact (regions with unsuppressed water signal) were estimated by prepending a water suppression module to a conventional imaging sequence. The combination of water-suppression imaging with SENSE-MRS reconstruction is termed estimation and removal of artifacts using sensitivity encoding ("ERASE").

2 | THEORY

2.1 | Signal unfolding

To separate spurious echo signals arising from distinct spatial regions, from a desired signal, the SENSE unfolding

approach is used.[11-14] In a K-channel receive array, the time-domain signal measured in the kth channel, C_k, can be expressed as a weighted sum of desired metabolite signal, x_V, from the voxel, V, and artifact signals, x_{A_j}, assumed to arise from N distinct regions, $\left(A_1, A_2, \ldots, A_N\right)$, such that

$$C_k = S_{V,k} x_V + \sum_{j=1}^{N} S_{A_j,k} x_{A_j} + \eta_k, \tag{1}$$

where η_k is the noise observed in channel k, and $S_{A_j,k}$ is the integrated receive sensitivity of the kth channel over the spatial region, A_j, defined as

$$S_{A_j,k} = \int_{\text{region}A_j} s_k\left(\vec{r}\right) d^3\vec{r}. \tag{2}$$

Here, $s_k\left(\vec{r}\right)$ is the complex sensitivity of the kth channel at position, $\vec{r}$. Equation 2 is also used to define $S_{V,k}$, calculated over the region encompassed by the voxel, V. In the unfolding approach, signals are assumed to be spatially homogeneous (ie, a single signal component in each region). Equation 1 can then be extended to a linear system of equations for all K receive channels, such that

$$\boldsymbol{C} = \boldsymbol{S}\boldsymbol{x} \tag{3}$$

where $\boldsymbol{x} = \left(x_V, x_1, \ldots x_N\right)^T$ are the signal components and $\boldsymbol{S}$ is the $K \times (N+1)$ sensitivity matrix. To separate the aliased signals, Equation 3 can be solved using the unfolding matrix, $\boldsymbol{U}$, given by[11]

$$\boldsymbol{U} = \left(\boldsymbol{S}^H \Psi^{-1} \boldsymbol{S}\right)^{-1} \boldsymbol{S}^H \Psi^{-1}. \tag{4}$$

Here, Ψ is the $K \times K$ noise covariance matrix of the receive array, and $\boldsymbol{S}^H$ is the conjugate transpose of the sensitivity matrix. Effective separation of multiple signals using receive-coil sensitivities relies on a unique weighting of each receive channel, at each location. Regions with similar channel sensitivities lead to poorly conditioned signal unfolding and noise amplification, which is dependent on the coil geometry. The SNR penalty of unfolding relative to the separate reconstruction of region, j, is expressed as the geometry factor (g-factor), g, such that

$$g_j^2 = \left(\boldsymbol{S}^H \Psi^{-1} \boldsymbol{S}\right)_{j,j}^{-1} \left(\boldsymbol{S}^H \Psi^{-1} \boldsymbol{S}\right)_{j,j}. \tag{5}$$

Equation 5 is identical to previous SENSE approaches to multivoxel MRS,[14,19] because the unfolding of artifact and metabolite signals can be considered as a form of accelerated parallel reconstruction of simultaneously excited signals.

2.2 | Quantifying removal

Similar to previous sensitivity-based approaches,[12,18] a spatial response function can be defined by applying the unfolding matrix (Equation 4) to each spatial point. In this way, the amount of signal (phase and amplitude) at $\vec{r}$ contributing to the unfolded spectrum from V can be calculated, such that

$$\text{SRF}_V\left(\vec{r}\right) = \sum_{k=1}^{K} U_{k,V} s_k\left(\vec{r}\right). \tag{6}$$

By integrating Equation 6 over some spatial region, R, a metric, ϑ_R, for assessing the total signal contribution to the unfolded spectrum at V from spatial region R is defined as

$$\vartheta_R = \int_{\text{region}R} \text{SRF}_V\left(\vec{r}\right) d^3\vec{r}. \tag{7}$$

It can be shown that when region R is identical to region V in Equation 7, then $\vartheta_V = 1$ (see An et al[18]). In other words, there is perfect reconstruction of signal from V. If region R is defined by artifact region, A_j, then it can be shown that $\vartheta_{A_j} = 0$ for $j = 1 \ldots N$, indicating perfect removal of signal from these regions in the reconstructed spectrum. These results hold, provided that the regions are known and coil sensitivities can be estimated. In addition, the signal model (Equation 1) assumes a single component in each region.

In practice, A_j is not known a priori; thus, the calculated unfolding matrix does not capture the sensitivities of the true artifact regions, in which case some degree of artifact signal will remain in the reconstructed spectrum, $\vartheta_{A_j} > 0$. Furthermore, due to the nature of the spurious echo artifact, there is likely heterogeneity in the signal in each estimated artifact region. However, the aim of this work is the removal of spurious echo contribution from the reconstructed metabolite spectrum, rather than accurately reconstructing each artifact signal. Thus, provided that the proposed method is effective in reducing the artifact signal contribution in metabolite spectra, it may prove sufficiently powerful for MRS even when signal-unfolding assumptions are not fully met. To assess the influence of these effects on artifact removal, the performance of the method is examined in simulation experiments and in vivo acquisition.

3 | METHODS

3.1 | Simulation of artifact removal

To assess the feasibility of the proposed sensitivity-based artifact removal method, simulations of single-voxel MRS acquisition with the addition of spurious echo artifact were

performed. A set of complex sensitivity maps were simulated using the Biot-Savart law, using a freely available toolbox for parallel MRI written in *MATLAB* (MathWorks, Natick, MA).[20] Signal reception was simulated using a 16-channel circular array of 30-cm diameter and 4-cm coil radius, over a 2D spatial grid of 256×256 mm^2 with 1×1 mm^2 resolution. A "ground truth" metabolite signal was modeled by density matrix simulations for a STEAM localized acquisition (TE = 14 ms) arising from a 2×2 cm^2 voxel. A single artifactual signal component was simulated as an echo-based complex exponential signal at a chemical shift value of 3.9 ppm, with a refocused echo occurring 164 ms after the start of signal reception and a transverse decay time, $T_2 = 20$ ms. The off-diagonal components of the simulated noise covariance were zero. For a list of simulation parameters used to generate the spurious echo artifact, see Supporting Information Text S1.

For data acquired in vivo, the spatial origin of spurious echo artifacts may not be known accurately, so it is important to understand how a mismatch between the estimated and actual artifact location affects the performance of the proposed method. Therefore, three sets of simulation experiments (experiments 1-3) were performed with different configurations of artifact and estimated reconstruction regions. In all cases, the location of the MRS voxel was fixed and assumed to be known. In experiment 1, the shape, size, and position of the artifact region was varied and subsequently reconstructed, assuming exact knowledge. In experiment 2, the shape, size, and position of the artifact region was fixed, whereas the "estimated" region for reconstruction (for calculation of Equation 2) was systematically varied across the whole 2D spatial grid. At each grid position, the signal contribution arising from the true artifact location was calculated using Equation 7. A total of 63 273 reconstructions were performed (excluding region estimates that overlapped with the MRS region). In experiment 3, an additional ground-truth artifact was simulated in a region adjacent to the first, with different signal characteristics (3.5 ppm, $T_2 =$ 2 ms, occurring 492 ms into signal reception). The removal performance was compared using knowledge of all regions, using only one region, and using a single estimated region encompassing both ground-truth artifact regions to simulate the effect of nonuniformity within a region.

3.2 | Magnetic resonance spectroscopy acquisition

Experimental data were acquired with 5 healthy volunteers (mean age = 33 years, 1 female, 4 male) on a 3T Philips Ingenia Elition MR system (Amsterdam, Netherlands) with 32-channel receive array head coil. All participants provided written, informed consent, as approved by the Johns Hopkins Medicine Institutional Review Board. A total of six data sets (R01-R06) were obtained from three brain regions: two in occipital cortex ($15 \times 15 \times 15$ mm^3; R04 and R06), one in putamen ($30 \times 15 \times 15$ mm^3; R02), and three in anterior cingulate cortex ($20 \times 20 \times 20$ mm^3 for R03 and R05 and $15 \times 15 \times 15$ mm^3 for R01). A T_1-weighted MPRAGE acquisition (TR = 13 ms, TE = 3.5 ms, 1-mm in-plane resolution) was additionally acquired for voxel placement.

The MR spectra were acquired using standard PRESS localization (TE/TR = 30/2000 ms) with VAPOR water suppression (bandwidth = 100 Hz). The pulse sequence diagram is shown in Supporting Information Figure S2. For test purposes, to increase the presence of spurious echo artifacts, no phase cycling was performed. In addition, projection-based shimming was carried out using up to second-order corrections, optimized over the same spatial extent as the observed voxel; this is known to increase field inhomogeneity in parts of the sample remote from the voxel, leading to increased spurious echoes. A total of 64 transients were acquired.

For assessment of the efficacy of the proposed ERASE method, comparisons were made to conventionally reconstructed multichannel data (termed here as "standard reconstruction"), which were calculated using the coil-sensitivity information at the target voxel and the measured noise covariance (equivalent to a SENSE-based weighted combination). After coil combination, individual transients were frequency-corrected and phase-corrected before being averaged.

3.3 | Calculation of coil sensitivities

Individual channel sensitivity maps were determined using a 3D gradient-echo acquisition (TE/TR = 0.97/4.1 ms, 3.5-mm isotropic resolution, acquisition time = 43 seconds). Complex channel sensitivities were calculated using ESPIRiT[21] as part of the BART Toolbox for computational MRI,[22] using the raw k-space data exported from the scanner. The complex noise covariance between the 32 receive channels was calculated using raw noise samples obtained on each channel as part of the scanner's preparation steps before acquisition of the gradient-echo image data. For the unfolding of spectral and artifact signals from multiple regions, coil sensitivities were calculated as the sum of the sensitivities within the MRS voxel or estimated artifact regions of interest (Equation 2).

3.4 | Spectral fitting

To compare the performance of artifact removal using either the ERASE method or standard coil combination, spectra were fit using LCModel.[23] A basis set was generated using

2D density matrix simulations of PRESS acquisition (TE = 30 ms) of 19 commonly observed metabolites (namely, alanine, ascorbate, aspartate, creatine, gamma-amino butyric acid, glutamine, glutamate, *myo*-inositol, lactate, phosphocholine, phosphocreatine, phenylethyanolamine, *scyllo*-inositol, taurine, glucose, glycerophosphocholine, glutathione, N-acetylaspartate, and N-acetylaspartylglutamate). Estimated concentrations and Cramér–Rao lower bounds (CRLBs) of fitting were compared on spectra reconstructed using ERASE and standard coil combination. Because estimated concentration values were not the focus of this study, no corrections for T_2 relaxation times were applied. Data sets R04, R03, and R06 were fit over the range 1.8 ppm to 4.2 ppm due to severe lipid contamination, whereas the remaining data sets were fit over the range of 0.5 ppm to 4.2 ppm.

Raw SNR was measured in the spectral domain as the height of the NAA peak at 2.01 ppm divided by the SD of the noise in the range of 15-20 ppm using the FID-A toolbox.[24] In addition, LCModel reported that SNR values were compared between ERASE and standard-coil combinations.

3.5 | Water-suppression imaging

The artifact is believed to originate in most cases from regions of the head where B_0-field inhomogeneity has shifted the water resonance outside of the bandwidth of the water-suppression pulses. Thus, to identify the location of the artifact signal in vivo, water-suppression imaging (WSI) maps were acquired using a modified sequence similar to that described in Carlsson et al.[4] The WSI maps were acquired after MRS using a 2D turbo spin-echo sequence (64 slices, 3.5-mm isotropic resolution, TE = 160 ms, TR = 3 seconds, acquisition time = 2:27 minutes) and included a VAPOR water-suppression preparation module (RF pulse bandwidth = 100 Hz). Importantly, WSI was performed with the identical first-order and second-order shim settings, in addition to water-suppression parameters, as those used to acquire the MRS signal. In addition, a whole-brain B_0 field map (TR = 8.2, TE = 3.3 and 5.6 ms, 3.5-mm isotropic, acquisition time = 1:06 minutes) was acquired after MRS acquisition using identical shim settings for validation of the WSI method.

3.6 | Estimation of artifact regions

To determine regions that are solely influenced by water suppression, and to remove tissue contrast from the images, a residual WSI (rWSI) approach was developed by normalizing the WSI images to an identical acquisition acquired without water suppression (non-WSI). An automated algorithm was developed to subsequently partition binary rWSI maps (thresholded at the mean image intensity of nonzero voxels) into separate artifact regions for reconstruction. Regions were segmented and labeled by iteratively eroding the rWSI maps and then applying a watershed transform[25] to generate unique contiguous regions based on nearest-neighbor distances. The watershed transform was chosen, as it is able to segment connected regions into smaller subregions. The region-segmentation algorithm was implemented in *MATLAB*. This iterative process continued until eight or fewer possible artifact regions were identified. Regions were also constrained to be bigger than a single image voxel; however, no constraint was placed on the maximum region size.

4 | RESULTS

4.1 | Effect of artifact size and location

A demonstration of the proposed method for artifact removal is shown in a numerical phantom (Figure 1) for regions of different size, shape, and location (experiment 1). The phantom contained a simulated metabolite signal originating from the MRS region (V) and a single simulated spurious echo artifact component (centered on 3.9 ppm) originating from a region (A). The center of A was varied to lie (1) 6.5 cm, (2) 10 cm, and (3) 5.3 cm from V, and its total area was calculated to be 7.2 cm^2, 49.7 cm^2 and 1 cm^2, respectively. Coil combination of the resulting multichannel data using standard reconstruction resulted in considerable contamination of the metabolite spectrum by the spurious echo in all cases (Figure 1A-C). Under ideal simulated conditions of a single uniform artifactual signal and exact knowledge of the artifact region, A, the proposed ERASE reconstruction method resulted in unfolded signal components with clear separation of metabolite and artifact signal (Figure 1H-J), thereby completely removing artifact from the metabolite spectrum. Maps of the spatial response function of the reconstructed metabolite signal (SRF_V) (Figure 1E-G) show the signal weighting over the numerical phantom during unfolding. In particular, there was a 2π phase cancelation of signal over region A, in addition to a lower signal magnitude at the center of A. As a result, the integral of SRF_V (Equation 7) calculated over A, $|\vartheta_A|$, was 0 for all configurations.

4.2 | Effect of region estimation

For data acquired in vivo, the spatial origin of spurious echo artifacts may not be known accurately, so it is important to understand how mismatch between the estimated and actual

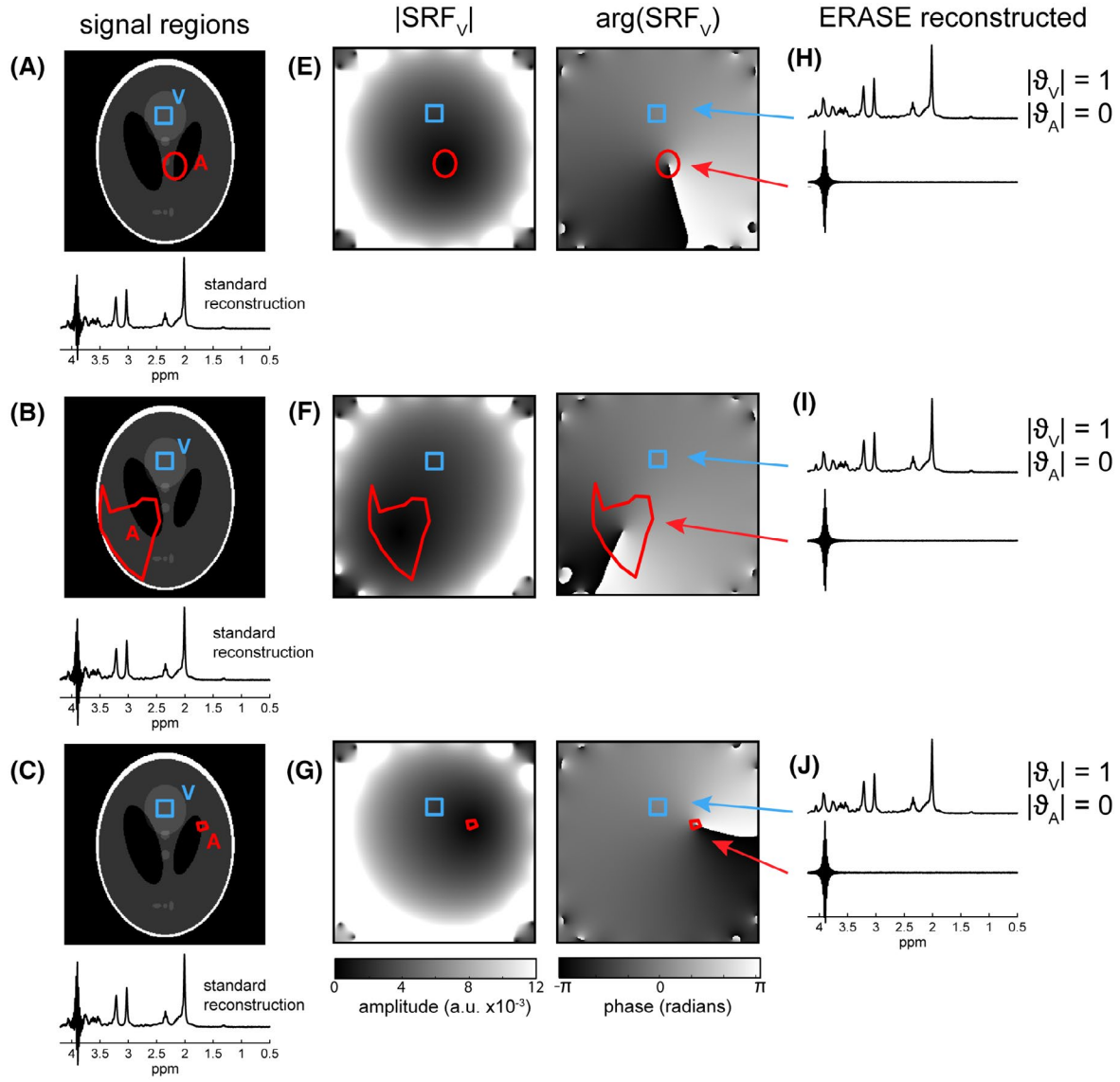

FIGURE 1 Numerical phantom simulations of the proposed artifact-removal method for different sizes and locations of artifact regions (experiment 1). A metabolite spectrum (STEAM, TE = 14 ms) was simulated to arise from an MRS region (V; blue) and a spurious echo artifact (at 3.9 ppm) from region A (red). A-C, The artifact support region is varied, and the coil-combined data using standard reconstruction is shown. E,F, The corresponding complex-valued spatial response function (SRF_V) (Equation 6) resulting from the "ERASE" (estimation and removal of artifacts using sensitivity encoding) reconstruction. H-J, The corresponding unfolded spectra using ERASE reconstruction. In all cases, there was complete removal of artifact from the metabolite spectrum, as indicated by the integral of the SRF_V over A, $|\vartheta_A| = 0$

artifact region affects the performance of the ERASE method. Figure 2 shows the numerical phantom results obtained after varying the location of the reconstruction region, while keeping the size and position of the true artifact region fixed (Figure 2A). As the "estimated" region moved further from the true region, A, the removal performance deteriorated. The proportion of artifact signal in the unfolded metabolite spectrum (Figure 2B) was below one for small errors in the estimated region, indicating partial removal. In extreme cases, when the reconstruction region was positioned far from the true artifact region, there was worse performance than standard combination ($|\vartheta_A| = 1.77$; Figure 2C,D), leading to an increase in the proportion of artifact signal. These simulations illustrate the importance of accurately identifying the location of the artifact signal in order for it to be successfully eliminated using ERASE. Importantly, even when the reconstruction location was not aligned with the ground truth, there was still a perfect reconstruction of metabolite signal from V (ie, $|\vartheta_V| = 1$) in all cases.

4.3 | Effect of multiple artifacts

With the inclusion of an additional artifact (centered at 3.5 ppm) from a second region, A_2, standard reconstruction led to considerable contamination from both artifacts (Figure 3A).

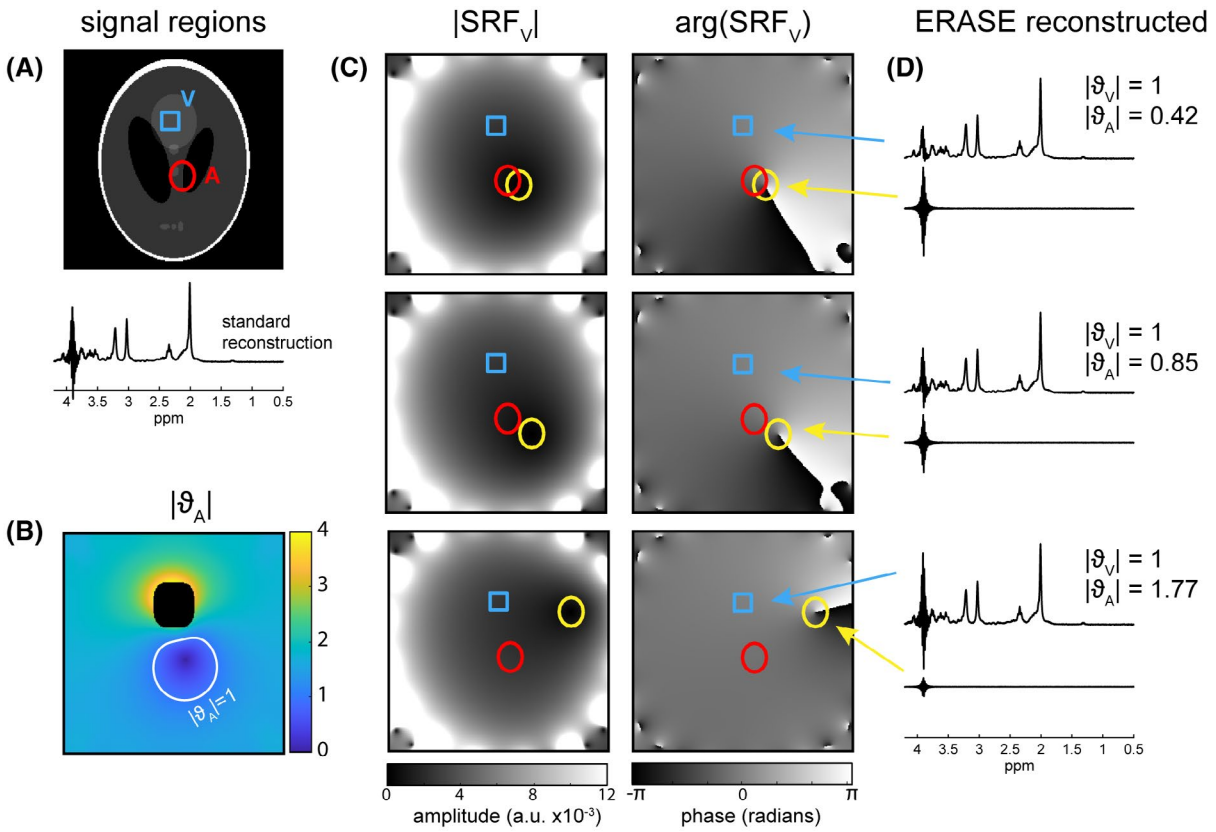

FIGURE 2 Simulations of the effect of estimating the position of the artifact region on removal performance (experiment 2). A, The simulated ground-truth configuration of MRS voxel (*V*; blue) and artifact region (*A*; red), together with standard reconstruction. B, Heatmap showing the magnitude of the signal contribution in the metabolite spectrum from the true artifact region *A* as the reconstruction region is placed at each point in the phantom. The white contour line shows where there is no removal (ie, $|\vartheta_A| = 1$). C,D, The SRF_V and reconstructed spectra from three points in the phantom. The "estimated" reconstruction region is shown in yellow

As expected, removal of artifact signal was complete $\left(|\vartheta_V| = 1, \left|\vartheta_{A_1}\right| = 0, \left|\vartheta_{A_2}\right| = 0\right)$ when both true artifact regions were used for reconstruction (Figure 3B,E). If only a single artifact component was assumed by reconstructing at A_1, then the additional artifact at A_2 was partially removed (Figure 3C,F) in the ERASE-reconstructed metabolite spectrum $\left(\left|\vartheta_{A_2}\right| = 0.25\right)$. Finally, when a single reconstruction region encompassed both true artifact regions, then ERASE reconstruction was able to partially remove contributions from A_1 and A_2 with $\left|\vartheta_{A_1}\right| = 0.26$ and $\left|\vartheta_{A_2}\right| = 0.16$, and generated a considerably cleaner metabolite spectrum than standard reconstruction (Figure 3D,G).

4.4 | Water suppression imaging and artifact-region estimation

For the estimation of spatial origin of artifacts in vivo, WSI maps were acquired in each volunteer. The WSI maps and corresponding rWSI maps, showing regions of unsuppressed water, are shown for 2 volunteers in Figure 4. The WSI maps, acquired using identical second-order shims to the MRS acquisition, was found to show regions of poor water suppression very clearly, indicated by higher signal intensity. In all acquisition geometries, there was unsuppressed signal in the oral cavity and adjacent structures, infratentorial regions, and other regions distal from the MRS acquisition voxel. Pericranial lipid signal was visible in all WSI images, as it lies outside the water-suppression bandwidth and is unaffected by the water-suppression module. Placing the MRS voxel in an anterior region (Figure 4A) led to large regions of unsuppressed water in the cerebellum and above the frontal sinus. Conversely, for the voxel positioned in the occipital region (Figure 4B), the frontal lobe contained a large area of unsuppressed water. The spatial distribution of the WSI images was observed to correspond strongly with the B_0 distribution after localized shimming. When normalized to the image acquired without water suppression and masked, rWSI maps could accurately reveal unsuppressed regions, without the underlying gray-matter and white-matter contrast observed in the WSI maps themselves.

The automated thresholding and segmentation procedure used in this work (Figure 5) resulted in separate contiguous regions of potential spurious echo artifact for each MRS region. The algorithm led to estimation of between two and eight regions.

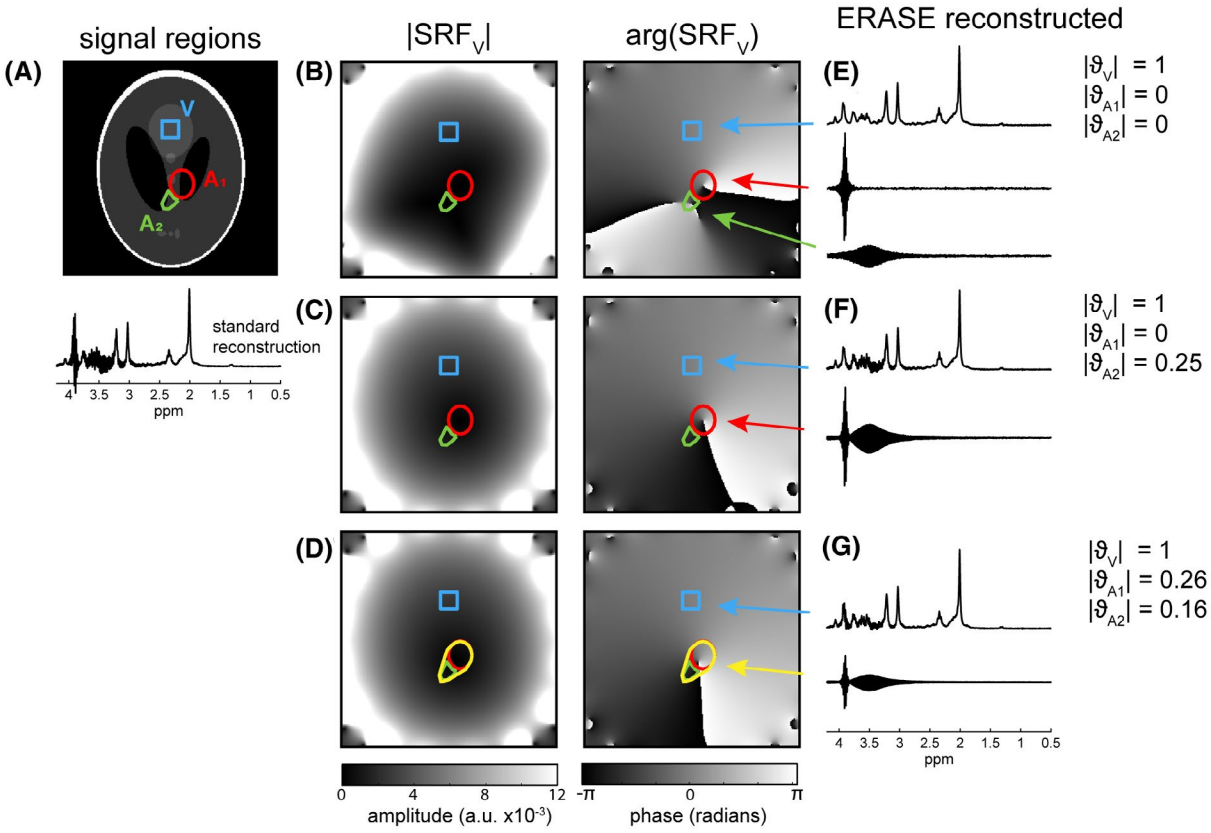

FIGURE 3 Simulations of the effect of multiple artifact signals on removal performance (experiment 3). A, The ground-truth configuration contains two adjacent artifact regions (A_1, red; A_2, green) and shows standard reconstruction with contamination of spectra between 3-4 ppm. Three different reconstructions are shown with SRF_V maps (B-D) and the corresponding ERASE-reconstructed spectra (E-G). Reconstruction using three signal components with precise knowledge of regions (B,E) shows perfect removal of artifact. Using a single region (A_1) in the reconstruction (C,F) resulted in the complete removal of one artifact ($|\vartheta_{A_1}| = 0$) and partial removal of the other ($|\vartheta_{A_2}| = 0.25$). Using a single region (yellow) containing both artifacts (D,G) resulted in partial removal of both spurious echo artifacts

There was a large variation in estimated region volume (mean ± SD: 57±111 cm^3, minimum: 0.086 cm^3, maximum: 573 cm^3).

4.5 | Spectral quality of reconstruction in vivo

Individual channel sensitivity maps, acquired in vivo and processed offline, were smoothly varying as expected: Representative data are provided in Supporting Information Figure S3. The ERASE reconstruction method in three data sets (R03, R06, and R02) is shown in Figure 6. The remaining three data sets are provided in Supporting Information Figure S4. Spurious echo artifacts were observed in all data sets and regions (apart from R05), and were largely centered over the 3-4 ppm region of the spectra.

Figure 6A shows artifact estimation and removal results for a voxel placed in the anterior cingulate cortex (R03). The rWSI maps revealed unsuppressed water signals in temporoparietal regions of both hemispheres, which were automatically segmented into two regions (A,B) and contributed relatively little artifact signal to the spectrum. Two further regions (C,D) adjacent to the frontal sinus were segmented and led to the largest reconstructed artifactual signal components dominated by a signal around 3 ppm. The reconstructed spectrum from the MRS voxel (V) using the ERASE method was visibly improved compared with the standard method, particularly in the 3-4 ppm region. The appearance of the mI peaks was visibly improved.

Figure 6B shows the results for a voxel in the occipital cortex (R06). The rWSI maps revealed an area of unsuppressed water in the frontal lobe, which was automatically segmented into three regions (A-C) in addition to a small region near frontal sinus (D) and two more regions inferior to the MRS region in temporal lobe (EE) and cerebellum (F). The reconstructed MRS spectrum using the ERASE method was much cleaner than the standard reconstruction. In particular, there was a cleaner appearance of the mI peaks, and complete removal of a spurious peak around 3.3 ppm. The difference between both reconstructions (labeled "residual" in Figure 6) showed no removal of metabolite peaks with ERASE. Lipid contamination was equally present in both the standard and ERASE reconstructions, as expected, as no attempt was made to unfold pericranial lipid signals. The temporal lobe region (E) contained relatively little artifactual signal, whereas frontal regions (A) had larger high-frequency artifactual component (>3.5 ppm).

Figure 6C shows the voxel acquired in the putamen (R02). Standard reconstruction resulted in severe contamination

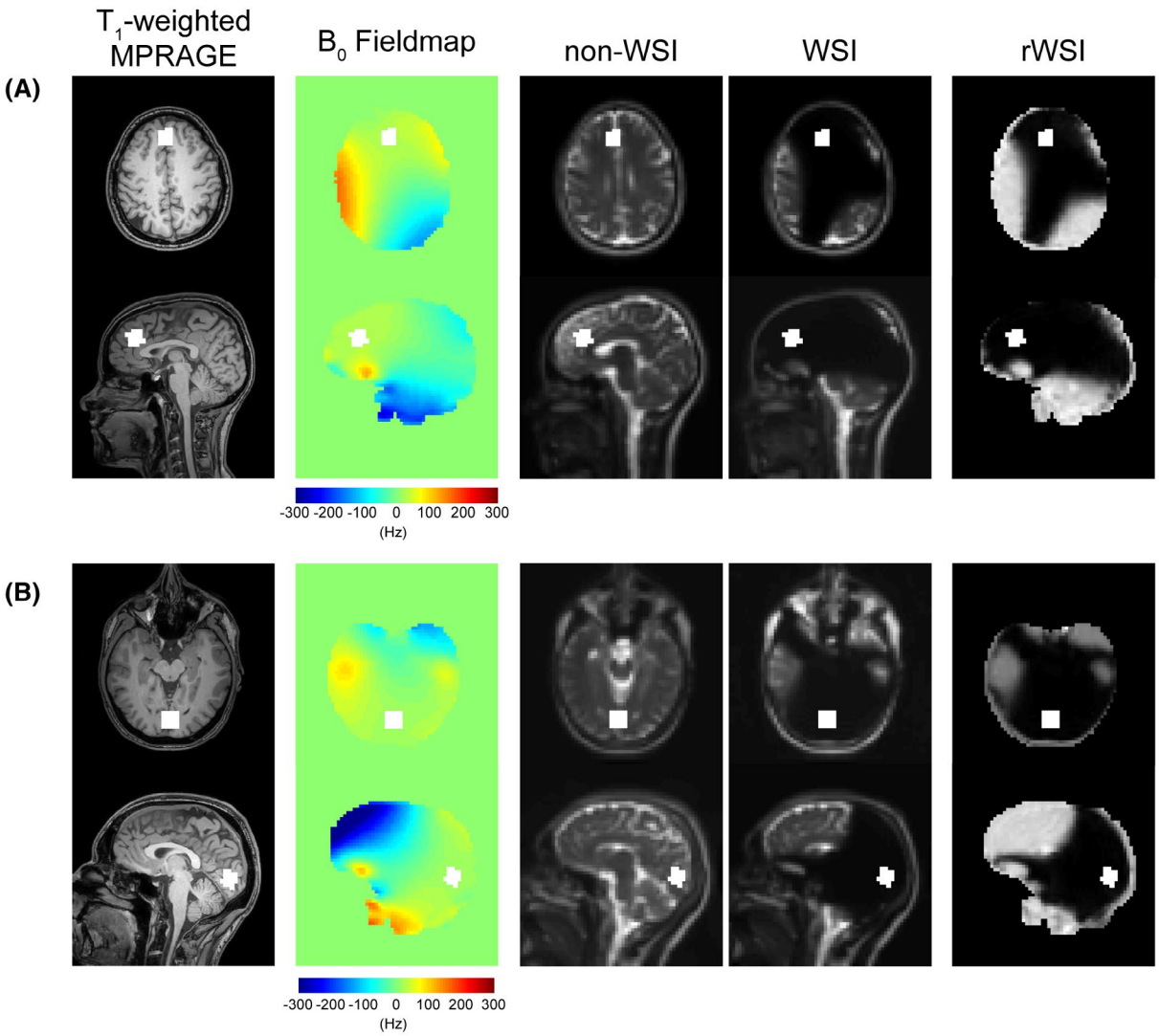

FIGURE 4 Water-suppression imaging (WSI) for identification of spurious echo artifact regions. Data shown for data sets in anterior cingulate cortex (A) and occipital cortex (B). The MRS voxel position is the white box overlaid onto the anatomical T_1-weighted scan, B_0 field map, WSI, with and without water suppression (non-WSI). The residual WSI (rWSI) is formed by normalizing the WSI to non-WSI and masking. Note the high similarity between rWSI and B_0 field map

around the choline peak at 3.2 ppm and total creatine peak at 3.9 ppm. Artifactual components were primarily estimated to arise from regions (A,B) both anterior and posterior to the MRS voxel, with large signal over the 3-4 ppm range. The ERASE reconstruction revealed a cleaner spectrum over this range, as shown by the improved shape of the choline and creatine peaks.

4.6 | The g-factor and SNR

The MRS voxel with the largest associated g-factor (Equation 5) of reconstruction was data set R01 (g = 2.75) in the frontal region with eight artifact regions estimated. This data set also had the largest spectral SNR penalty of reconstruction measured in the spectral domain (54.6 vs 25.3; standard vs ERASE); however, it still performed well in terms of artifact removal (Supporting Information Figure S4). A complete list of g-factors and corresponding measured spectral SNR is provided in Table 1. As expected, there was a linear relationship between the calculated g-factor for the MRS voxel and the measured SNR penalty following ERASE reconstruction ($SNR_{standard}/SNR_{ERASE}$), as measured using a regression analysis, but this was less than unity ($R^2 = 0.73$, $\beta = 0.6$, $P = .03$). The LCModel-reported SNR (which accounts for residual unfitted signal in its noise estimation) was significantly improved for ERASE reconstructed spectra than standard combination (8.8 vs 6.8; $P = .02$; paired t-test).

4.7 | Metabolite fitting

Spectra processed with standard combination and ERASE were fit using the LCModel. The difference in the CRLBs

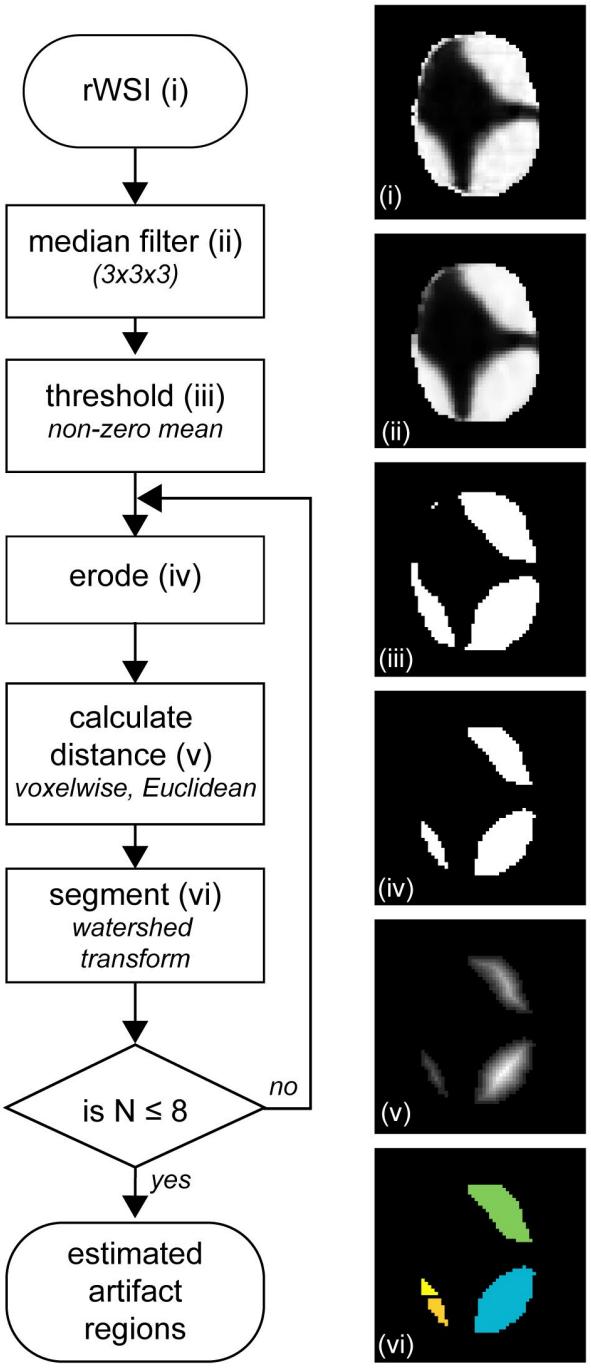

FIGURE 5 Flowchart outlining the steps (i-vi) in the artifact region segmentation algorithm using the rWSI acquired in vivo. After filtering and thresholding, images are eroded and segmented into separate regions using the watershed transform. This process is repeated until the number of estimated regions, *N*, is less than or equal to 8. Intermediate steps are shown using an example transverse slice (R02). In practice, the image-processing steps are applied to the 3D image data

between reconstructing with ERASE and standard reconstruction are shown in Figure 7A for five major metabolites. Across all six data sets, the CRLBs for total N-acetylaspartate, total choline, total creatine , glutamate plus glutamine, and *myo*-inositol using ERASE were less than or equivalent to standard combination. Fitting errors were significantly lower using ERASE compared with the standard combination for all major metabolites, apart from glutamate plus glutamine (11.7% vs 14.7%; $P = .06$), which was very close to significance: total N-acetyl aspartate (5.6% vs 7.0%; $P = .03$), total choline (10.7% vs 14.1%; $P = .019$), total creatine (7.0% vs 9.2%; $P = .04$), and mI (13.7% vs 17.5%; $P = .03$). The difference in estimated metabolite concentrations is also provided in Figure 7B. There was no clear difference in the metabolite concentrations after using ERASE reconstruction for the major metabolites across data sets, which was also confirmed statistically using a paired t-test. One data set (R05) saw no reduction in CRLBs and very little change in estimated concentration after ERASE. This data set also contained no clear spurious echo signal in its metabolite spectrum following standard reconstruction.

5 | DISCUSSION

An approach for the removal of spurious echo artifacts from single-voxel MR spectra is presented, based on receive-coil sensitivity profiles. As demonstrated by numerical simulations, the method works best when the spatial origin of spurious echoes is accurately known. In this study, rWSI was used to identify regions likely to contribute artifactual signal; under the conditions used here, frontal regions and the cerebellum were often found to have large amounts of residual water shifted outside the bandwidth of the water-suppression pulses. Across six in vivo data sets acquired in three different brain regions, the proposed ERASE method visibly improved spectral quality compared with standard reconstruction of multichannel MRS data, in particular over the 3-4 ppm region. Spectra reconstructed using ERASE showed lower fitting errors for all major metabolite resonances, reaching statistical significance for tNAA, tCr, tCho, and mI ($P < .05$; Figure 7). Despite the fact that sensitivity encoding has a g-factor-related penalty in SNR, the amount of any SNR reduction was below that attributed to the g-factor alone and did not hinder metabolite fitting in the current examples. It is anticipated that this method will be particularly useful for improving the quality of spectroscopic data when either gradient crushing power is limited, or other factors lead to significant out-of-voxel magnetization.

In theory, the ERASE method requires only receiver-coil sensitivity maps, which are frequently acquired as a calibration step during a standard MR protocol. Thus, the method could be applied post hoc to data where this information is available. However, unlike previous methods exploiting sensitivity-based unfolding in MRS, such as lipid removal in MRSI,[13] multivoxel localization[14] and SPLASH,[18] the spatial origin of the artifact

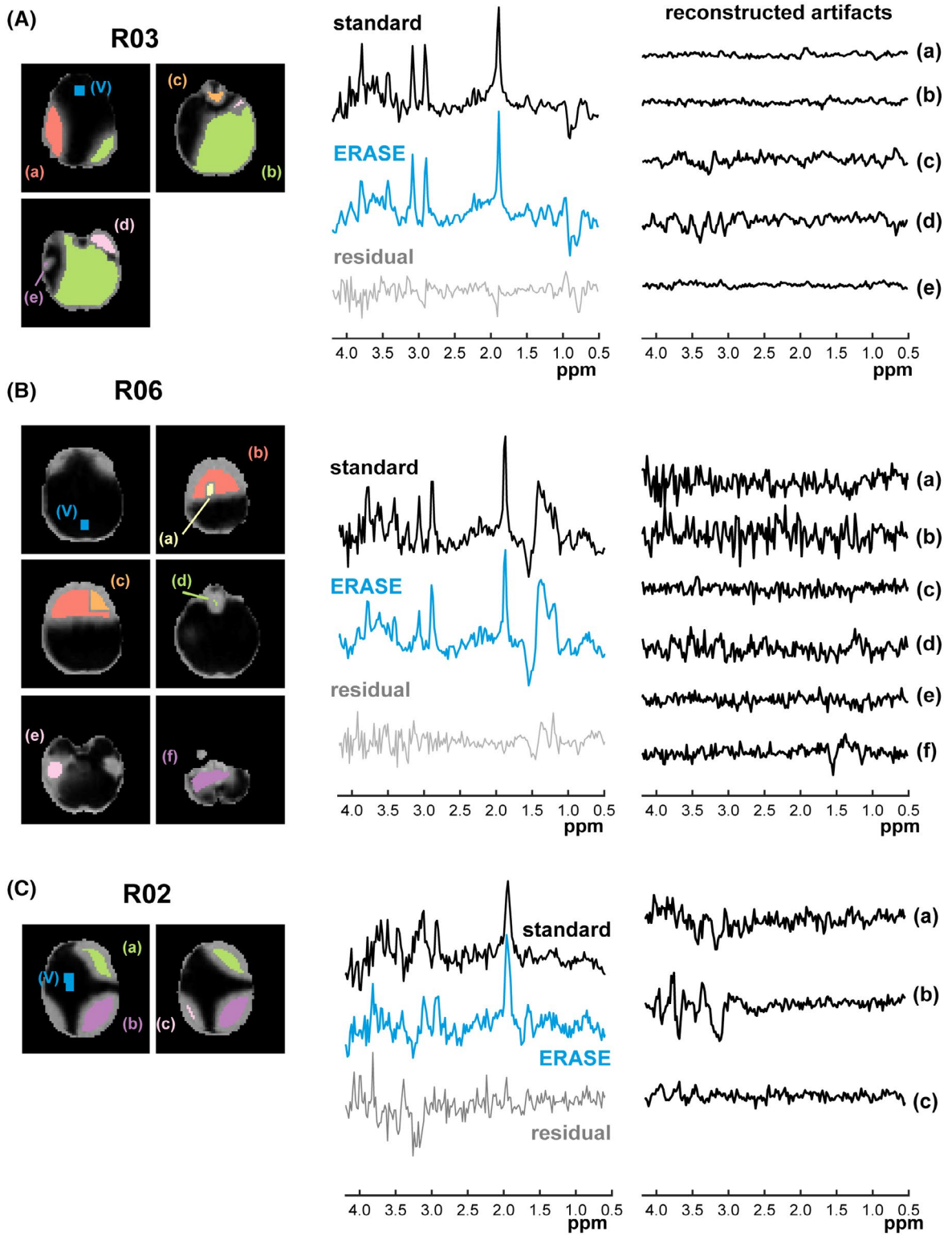

FIGURE 6 In vivo demonstration of the ERASE method in three data sets acquired in anterior cingulate cortex (A), occipital cortex (B), and putamen (C). Segmented artifact regions are overlaid in color and labeled (a-f) on the rWSI maps for each data set for different transverse image slices. The MRS voxel (*V*) is shown in blue. In each data set the standard reconstruction is shown above the ERASE reconstructed data for the voxel, V (blue). Alongside the metabolite spectra, the artifact spectra reconstructed in each region (A-F) is plotted

signal is unknown beforehand. For aliased signal components to be fully reconstructed (Equation 4), the spatial origin of signals must be known (Equation 2). The numerical phantom simulations confirmed that when the estimated reconstruction region intersects fully with the true artifact region, signal separation was complete, as in the case of PRIAM.[14] Critically

Data set	Location	Regions	$SNR_{standard}$	SNR_{ERASE}	$SNR_{standard}$/ SNR_{ERASE}	g-factor
R01	Frontal	8	54.6	25.3	2.16	2.75
R02	Putamen	3	28.6	23.2	1.23	2.32
R03	Frontal	5	87.2	74.4	1.17	1.79
R04	Occipital	2	42.9	39.5	1.09	1.16
R05	Frontal	4	76.3	89.6	0.85	1.14
R06	Occipital	6	42.5	36.8	1.15	1.56

TABLE 1 Measured SNR of the Metabolite Spectrum Using Standard Reconstruction and ERASE Reconstruction for All Data Sets

Note: The ratio of $SNR_{standard}/SNR_{ERASE}$ is provided alongside the calculated g-factor associated with the MRS voxel (Equation 5).

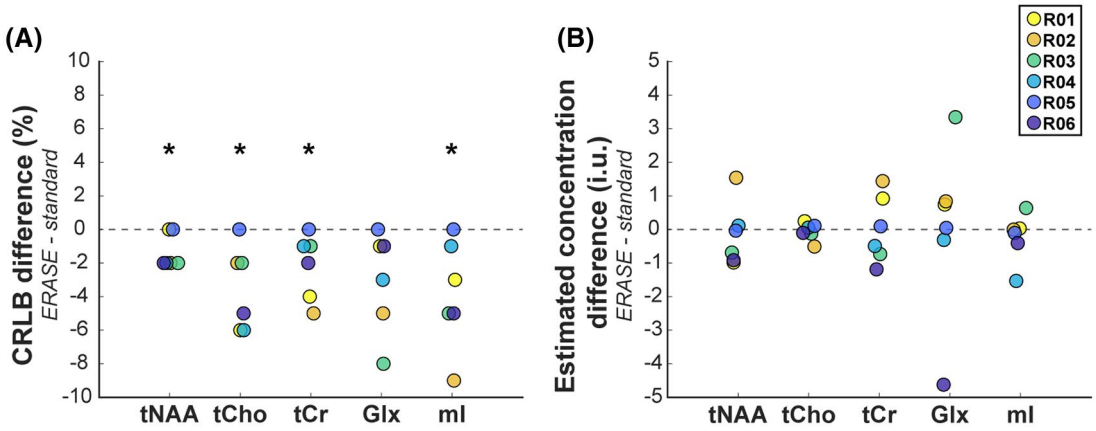

FIGURE 7 LCModel fitting results for major metabolite signals using standard and ERASE reconstructed spectra for all six in vivo data sets (R01-R06). A, Difference in the errors of fitting Cramér–Rao lower bounds (CRLBs) between ERASE and standard reconstructed data. Lower values indicate smaller CRLBs for ERASE. B, Difference in the estimated concentration values between ERASE and standard calculated relative to internal water reference. Values are in institutional units. *Indicates $P < .05$ after paired t-test. Abbreviations: Glx, glutamate plus glutamine; mI, *myo*-inositol; tCho, total choline; tCr, total creatine; tNAA, total N-acetylaspartate

for the success of ERASE, partial removal of artifact signal was achieved even when the reconstruction region did not fully overlap with artifact origin (Figure 2D), and when more than one signal component was present in a single region (Figure 3G). Importantly, the full metabolite signal from the MRS voxel was reconstructed in all cases, as measured using the spatial response function ($|\vartheta_V| = 1$), even when the artifact regions were not estimated correctly, thereby indicating no loss of metabolite signal using ERASE. This was also apparent in the in vivo data, whereby after applying ERASE reconstruction, there was no clear difference in estimated concentrations (Figure 7) or residual metabolite signal in the unfolded components (Figure 6). Under certain conditions, the true location of acquired metabolite signal may deviate slightly from the prescribed MRS voxel used for reconstruction, due to localization inaccuracy from chemical-shift displacement or imperfect excitation profiles. This effect may have a small influence on reconstructed metabolite signals, yet is present in all image-based techniques for MRS data reconstruction.

The WSI technique was relatively straightforward to implement and successfully mapped signal that was not suppressed by the water-suppression scheme, revealing potential regions of artifactual signal, similar to data presented in reference.[4] Scan time for WSI with whole-head coverage was about 2.5 minutes, limited primarily by the TR needed to incorporate the lengthy VAPOR sequence. Together with the non-water-suppressed image needed for calculating rWSI maps, the total WSI time was therefore 5 minutes. This could be dramatically reduced in future work, such as by reducing spatial resolution and using SENSE acceleration. In an MRS study involving multiple spectral locations (and hence multiple high-order shim settings), the WSI sequence will need to be repeated for each location. The WSI approach was chosen as a direct measurement of unsuppressed water, potentially accounting for differences in T_1 relaxation and B_1 transmit field across the brain. However, other approaches could also be considered for identifying regions of unsuppressed water, such as those based on B_0 maps, which showed good concordance with rWSI (Figure 4),and could be used if rWSI were not available on a particular scanner.

Across six data sets, independent of voxel geometry, unsuppressed water outside the volume of interest was often observed in frontal regions. This finding reflects previous work pointing to frontal sinuses and oral cavity as the main culprit for spurious

echo artifacts.[8] In addition, due to the use of localized high-order shimming, brain regions remote from the target voxel location often showed large amounts of unsuppressed water, often including the frontal or parietal lobes, and posterior fossa. These regions could potentially be reduced by the use of dynamic B_0 shimming, with a globally optimized shim set used during water suppression, and a regionally optimized shim set during data acquisition.[26,27] The WSI technique could potentially also be used online during scanning to plan acquisition-specific parameters such as order of slice-selection gradients or outer-volume saturation bands, to further reduce these artifacts. Removal of lipid signals was not considered in this work, as spurious echoes were anticipated to largely arise from unsuppressed water. However, by including known locations of lipid signal into the ERASE algorithm, their contribution to the spectrum could be removed similar to previous work using MRSI.[13]

The intensity thresholding and segmentation algorithm applied to rWSI maps generated a small number of volumes for ERASE reconstruction, which was limited to a maximum of eight regions. The theoretical maximum number of regions that can be reconstructed is limited by the total number of receive elements. However, a large number of volumes will generally decrease the conditioning of the unfolding matrix, and hence incur larger g-factor penalties associated with each region. This was observed in data set R01, where eight regions were identified ($g = 2.75$). In this work, low g-factors were measured for reconstruction of the MRS volume, presumably because artifact regions were generally far away from the target MRS volume. A linear relationship was found between g-factors and the ratio of SNR measured using ERASE and standard reconstructions ($\beta = 0.6$; $P = .03$), yet the influence of g-factor on reconstructed SNR was below the value predicted from SENSE unfolding alone ($\beta = 1$). This is likely due to two factors. First, some of the "noise" in the standard reconstruction actually results from very broad residual out-of-voxel signals that are removed by ERASE (Figure 3). Additionally, the height of the NAA peak used to determine SNR may be altered between reconstructions; in particular, an increase may occur if overlapping signal contributions with opposite phase are removed by ERASE.

As with similar compartment-based reconstruction methods, an assumption of unfolding is that of a single homogenous signal in each region. Unlike other methods,[18] however, accurate reconstruction of the artifact signals themselves is not required—just their removal from the metabolite spectrum. Our phantom results show that partial removal still occurs if the estimated region encompasses more than one unwanted signal. However, large region estimates are likely to contain multiple unwanted signals and worsen the g-factor penalty. In this work, the in vivo automated region estimation algorithm did not constrain maximum size, which led to large variation in region volumes (0.09-573 cm^3). Furthermore, the iterative erosion and watershed transform (Figure 5) led to heterogeneity in artifact size and shape across data sets. It is suggested that more sophisticated algorithms for region estimation could be implemented, based on a combination of region-growing and optimization by iterating ERASE reconstruction. Constraints could be placed on the total volume size, larger volumes split into subvolumes, and removal of regions found to contribute no artifact signal. Additionally, prior knowledge could be incorporated, such as the location of the slice-selection planes for each axis and sequence-specific coherence generation,[9] to improve region estimation.

This study has several limitations, including a lack of comparison to other methods for removing out-of-voxel artifacts in MRS data, such as the use of optimal crusher gradient schemes, or phase cycling. Future work will be required to establish whether the ERASE reconstruction method may be useful for data recorded in conjunction with such acquisition-related strategies.

6 | CONCLUSIONS

A new method for reconstruction and removal of spurious echo signals arising from out-of-voxel magnetization is demonstrated. Estimation of the artifact regions was achieved using an imaging-based method, and overlapping signal contributions were separated using sensitivity-based reconstruction. This method may improve quantification of metabolites when hardware limitations and voxel geometries lead to contamination of spectra, and could be modified in the future to be run as part of a standard MRS prescan.

ACKNOWLEDGMENT

The authors thank Dr. Georg Oeltzschner for the helpful discussion. A.B. also acknowledges the support of the Precision Imaging Beacon, University of Nottingham.

DATA AVAILABILITY STATEMENT

The numerical phantom and example code for the ERASE method are available at github.com/aberrington/ERASE.

ORCID

Adam Berrington https://orcid.org/0000-0002-1207-8193
Michal Považan https://orcid.org/0000-0002-5498-5162
Peter B. Barker https://orcid.org/0000-0002-6410-7793

TWITTER

Adam Berrington @adamberrington

REFERENCES

1. Kreis R. Issues of spectral quality in clinical 1H-magnetic resonance spectroscopy and a gallery of artifacts. *NMR Biomed.* 2004;17:361-381.

2. Moonen CT, Sobering G, Van Zijl PC, Gillen J, Von Kienlin M, Bizzi A. Proton spectroscopic imaging of human brain. *J Magn Reson*. 1992;98:556-575.
3. Starck G, Carlsson A, Ljungberg M, Forssell-Aronsson E. k-Space analysis of point-resolved spectroscopy (PRESS) with regard to spurious echoes in in vivo (1)H MRS. *NMR Biomed*. 2009;22:137-147.
4. Carlsson A, Ljungberg M, Starck G, Forssell-Aronsson E. Degraded water suppression in small volume ^{1}H MRS due to localised shimming. *MAGMA*. 2011;24:97-107.
5. Lei H, Xin L, Gruetter R, Mlynárik V. Localized single-voxel magnetic resonance spectroscopy, water suppression, and novel approaches for ultrashort echo-time measurements. In: Stagg C, Rothman D, eds. *Magnetic Resonance Spectroscopy*. Amsterdam, Netherlands: Elsevier; 2014:15–30.
6. Scheenen TWJ, Heerschap A, Klomp DWJ. Towards 1H-MRSI of the human brain at 7T with slice-selective adiabatic refocusing pulses. *Magn Reson Mater Phys Biol Med*. 2008;21:95-101.
7. Öz G, Tkáč I. Short-echo, single-shot, full-intensity proton magnetic resonance spectroscopy for neurochemical profiling at 4 T: validation in the cerebellum and brainstem. *Magn Reson Med*. 2011;65:901-910.
8. Ernst T, Chang L. Elimination of artifacts in short echo time ^{1}H MR spectroscopy of the frontal lobe. *Magn Reson Med*. 1996;36:462-468.
9. Landheer K, Juchem C. Dephasing optimization through coherence order pathway selection (DOTCOPS) for improved crusher schemes in MR spectroscopy. *Magn Reson Med*. 2019;81:2209-2222.
10. Kyathanahally SP, Döring A, Kreis R. Deep learning approaches for detection and removal of ghosting artifacts in MR spectroscopy. *Magn Reson Med*. 2018;80:851-863.
11. Pruessmann KP, Weiger M, Scheidegger MB, Boesiger P. SENSE: sensitivity encoding for fast MRI. *Magn Reson Med*. 1999;42:952-962.
12. Dydak U, Weiger M, Pruessmann KP, Meier D, Boesiger P. Sensitivity-encoded spectroscopic imaging. *Magn Reson Med*. 2001;46:713-722.
13. Ozturk-Isik E, Crane JC, Cha S, Chang SM, Berger MS, Nelson SJ. Unaliasing lipid contamination for MR spectroscopic imaging of gliomas at 3T using sensitivity encoding (SENSE). *Magn Reson Med*. 2006;55:1164-1169.
14. Boer VO, Klomp DWJ, Laterra J, Barker PB. Parallel reconstruction in accelerated multivoxel MR spectroscopy. *Magn Reson Med*. 2015;74:599-606.
15. Hurd R, Sailasuta N. Elimination of artifacts in short echo proton spectroscopy. In: Proceedings of the 5th Annual Meeting of ISMRM, Vancouver, Canada, 1997. p 1453.
16. Ernst T, Chang L. Elimination of artifacts in short echo time 1H MR spectroscopy of the frontal lobe. *Magn Reson Med*. 1996;36:462-468.
17. Li N, An L, Johnson C, Shen J. Phase-encoded single-voxel magnetic resonance spectroscopy for suppressing outer volume signals at 7 Tesla. *Biomed Spectrosc Imaging*. 2017;6:101-110.
18. An L, Warach S, Shen J. Spectral localization by imaging using multielement receiver coils. *Magn Reson Med*. 2011;66:1-10.
19. Oeltzschner G, Puts NAJ, Chan KL, Boer VO, Barker PB, Edden RAE. Dual-volume excitation and parallel reconstruction for J-difference-edited MR spectroscopy. *Magn Reson Med*. 2017;77:16-22.
20. Guerquin-Kern M, Lejeune L, Pruessmann KP, Unser M. Realistic analytical phantoms for parallel magnetic resonance imaging. *IEEE Trans Med Imaging*. 2012;31:626-636.
21. Uecker M, Lai P, Murphy MJ, et al. ESPIRiT—an eigenvalue approach to autocalibrating parallel MRI: where SENSE meets GRAPPA. *Magn Reson Med*. 2014;71:990-1001.
22. Uecker M, Tamir J. *Berkeley Advanced Reconstruction Toolbox (BART)*. 2019. doi:10.5281/zenodo.592960.
23. Provencher SW. Estimation of metabolite concentrations from localized in vivo proton NMR spectra. *Magn Reson Med*. 1993;30:672-679.
24. Simpson R, Devenyi GA, Jezzard P, Hennessy TJ, Near J. Advanced processing and simulation of MRS data using the FID appliance (FID-A)—an open source, MATLAB-based toolkit. *Magn Reson Med*. 2017;77:23-33.
25. Meyer F. Topographic distance and watershed lines. *Signal Process*. 1994;38:113-125.
26. Juchem C, de Graaf RA. B0 magnetic field homogeneity and shimming for in vivo magnetic resonance spectroscopy. *Anal Biochem*. 2017;529:17-29.
27. Boer VO, Andersen M, Lind A, Lee NG, Marsman A, Petersen ET. MR spectroscopy using static higher order shimming with dynamic linear terms (HOS-DLT) for improved water suppression, interleaved MRS-fMRI, and navigator-based motion correction at 7T. *Magn Reson Med*. 2020;84:1101-1112.
28. Lei H, Xin L, Gruetter R, Mlynárik V. Localized single-voxel magnetic resonance spectroscopy, water suppression, and novel approaches for ultrashort echo-time measurements. In: Stagg C, Rothman D, eds. *Magnetic Resonance Spectroscopy*. Amsterdam, Netherlands: Elsevier; 2014:15–30.

SUPPORTING INFORMATION

Additional Supporting Information may be found online in the Supporting Information section.

TEXT S1 Description of the simulation parameters used to generate spurious echo artifact signals

FIGURE S2 Pulse sequence diagram of the single voxel symmetric PRESS sequence used for the in vivo acquisitions. Sequence parameters were as follows: TE/TR = 30/2000 ms; samples = 2048, spectral width = 5 kHz. Around each refocusing pulse, the spoiler gradient pairs are shown

FIGURE S3 Example 32-channel receive sensitivity maps acquired and processed for one dataset in one subject (R06); a single axial slice at the level of the MRS voxel is shown. Data were processed with BART toolbox and are smoothly varying. Absolute values of the complex sensitivities are shown

FIGURE S4 ERASE reconstruction from remaining 3 datasets showing estimated artifact regions and reconstructed artifact spectra compared to standard reconstruction

How to cite this article: Berrington A, Považan M, Barker PB. Estimation and removal of spurious echo artifacts in single-voxel MRS using sensitivity encoding. *Magn Reson Med*. 2021;00:1–14. https://doi.org/10.1002/mrm.28848